Evolution of Laser-Induced Plasma during Radio-Frequency Plasma-Assisted Pulsed Laser Ablation of Titanium

E. Pajootan[1,2], F. Artistizabal[1], S. Coulombe[1] and S. Omanovic[2]

[1]*Plasma Processing Laboratory (PPL), Department of Chemical Engineering, McGill University, Montreal, Quebec, Canada*
[2]*Electrochemistry and Corrosion Laboratory, Department of Chemical Engineering, McGill University, Montreal, Quebec, Canada*

Abstract: We report on a preliminary study of the expansion dynamics of a titanium metal vapor plume produced by nanosecond-pulsed ablation of a solid target, in the presence or absence of a low-pressure capacitively-coupled radio-frequency plasma. We used high-speed imaging to monitor the plasma emission, and scanning electron microscopy to investigate the produced deposits collected on MWCNTs. We observed an effect of the background gas pressure (0.03 and 1.00 Torr, N_2) and presence of the continuous RF plasma (30 W) on the plasma emission and plume dynamics, as well as the coating morphology.

Keywords: nanostructured coatings, pulsed laser ablation, radio-frequency plasma, high-speed videography, coating morphology.

1. Introduction

The beneficial properties of titanium-based coatings and nanoparticles such as high conductivity and corrosion resistance have made titanium nitride (TiN) and titanium oxynitride (TiO_xN_y) thin films highly desirable in energy conversion and storage applications [1, 2]. The thermodynamically favourable formation of the native oxide/oxynitride layer on the surface of these coatings prevents further oxidation, and results in improved stability and durability of electrocatalysts [3, 4].

In this study, a combination of a nanosecond pulsed laser ablation (PLA) with a capacitively-coupled radio frequency (CCRF) plasma called radio-frequency plasma-assisted pulsed laser ablation (RF-PAPLA) was used to synthesize TiO_xN_y coatings on multiwalled carbon nanotubes (MWCNTs). The interaction of the radio frequency plasma with the laser-induced plasma containing ground- and excited-state neutral atoms, ions and electrons is known to affect the morphology, roughness and composition of the deposited layers [5]. Therefore, high-speed videography of the plasma formed during the ablation process was performed. The evolution of the laser-produced plasma and its expansion dynamics were investigated in an attempt to explain the different morphologies synthetized when comparing the PLA and RF-PAPLA processes.

2. Experimental

Fig. 1 presents the experimental setup. It consists of two vacuum chambers which can be isolated using a common gate valve. The left-end chamber is used for sample manipulation (substrate), while the right-end chamber is used for the RF-PAPLA setup (target). A high purity titanium target (99.95%, *Ted Pella Inc.*) mounted on a 9 cm O.D. stainless steel disc was ablated by a Quantel Brilliant B10 (Nd:YAG, 355 nm wavelength, 2.36 ± 0.01 Jcm^{-2} fluence, 10 Hz frequency and 4-6 ns pulse duration). The substrate used was a CVD-grown MWCNTs-covered stainless steel mesh mounted on a 6 cm O.D. stainless steel disc [6]. The target was also the live RF electrode while the substrate acted as the ground electrode. The target-to-substrate distance was set to 3 cm in all experiments. The experiments were carried out in nitrogen atmosphere at 0.03 and 1.00 Torr. A continuous RF signal (13.56 MHz and 30 W power) between the target and substrate holding plates was applied during the RF-PAPLA experiments.

A high-speed camera (Photron FASTCAM SA5, model 1000K-M1, monochromatic) was used to study the expansion dynamics of the pulsed laser ablation plasma plume. An arbitrary function generator (Tektronix-AFG3102) was used to trigger the Q-switch and the camera at prescribed delays with respect to the flashlamp output signal. The laser Q-switch was externally triggered with a 215 μs delay, while the camera delay was varied between 214 and 614 μs (20 ns increments) to cover the entire laser plume expansion event. A total of 64 frames (896 by 848 pixels) at 1 μs exposure were captured at any given camera time delay. The frames were then accumulated to produce an average image of the expanding plasma plume, frozen in time, at the corresponding camera delay.

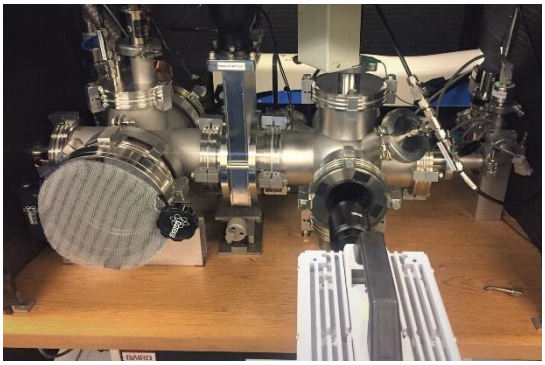

Fig. 1. Experimental setup during the videography of the RF-PAPLA: left chamber is the loading chamber and the right chamber is the RF-PAPLA.

3. Results and discussions

Scanning electron microscopy (SEM) images showing different morphologies of titanium nanostructures collected on MWCNTs are shown in Fig. 2. Particle decorated structures are obtained with PLA and RF-PAPLA at 1.00 Torr, while a dense coating of the MWCNTs is obtained at 0.03 Torr. The structures obtained at 1.00 Torr using PLA are decorated with nanoparticles, while the particles obtained when ablating with the RF plasma active (RF-PAPLA) are in the micrometer range. Structural differences are also observed when comparing PLA and RF-PAPLA processing at 0.03 Torr, where the layer-by-layer coverage of MWCNTs is more prominent and qualitatively larger structures are observed when the RF plasma was active.

The evolution of the laser-induced plasma plume expansion for PLA and RF-PAPLA at the two pressures studied are presented in Fig. 3 (three left-most columns). The laser/solid interaction results in the sublimation of the surface layer of the titanium target, which is followed by the laser/vapor interaction. As a result, an expanding plasma is formed. At the lower pressure (0.03 Torr), the plasma expands freely, while at the higher background gas pressure (1.00 Torr), there is a strong interpenetration of the laser-produced metal vapor plasma plume and surrounding N_2 gas. This enhances the collisions on the expansion front and inter-plume regions, which results in an increase of fluorescence from all species, as observed in Fig. 3. Higher intensity regions in Fig. 3 showed by color red correspond to areas of high temperature and/or high particle density in the plasma plume [7]. Plasma emission is observed up to 2 μs at 0.03 Torr and 8 μs at 1.00 Torr (results not shown). The plasma plume expansion process is similar for PLA and RF-PAPLA, as illustrated in Fig. 3 by comparing rows at similar pressures with and without RF plasma. The expansion process is significantly different at the two pressures studied, thus explaining the large morphological changes with pressure indicated in Fig. 2.

The right-most column in Fig. 4 corresponds to time delays of 30 μs (for 0.03 Torr) and 400 μs (for 1.00 Torr) after the end of the laser ablation pulse. At this point in time speckles are captured by camera (50 μs exposure time). We attribute these speckles to droplet ejection from the localized erosion of the titanium target by the laser pulse. These droplets are ejected at temperatures between the melting and boiling point of titanium (1941 K to 3560 K) and emit blackbody-like radiation visible to the camera. The main difference before and after applying the RF plasma is observed at longer time delays after the laser pulse, when the droplets ejection happens. Lower emission intensities were recorded at both pressures (0.03 and 1.00 Torr) when RF plasma was applied. Therefore, the morphological differences obtained between PLA and RF-PAPLA processing indicated in Fig. 2 could be explained by the carefully studying the changes in the droplet ejection process with and without the RF plasma.

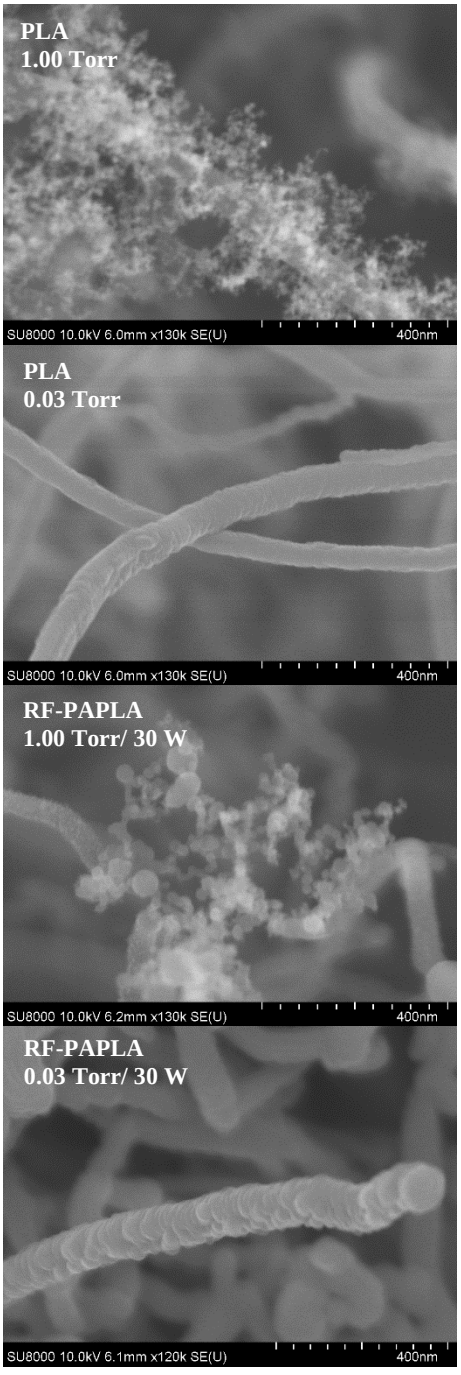

Fig. 2. SEM images of titanium nanostructures deposited on MWCNTs at different experimental condition.

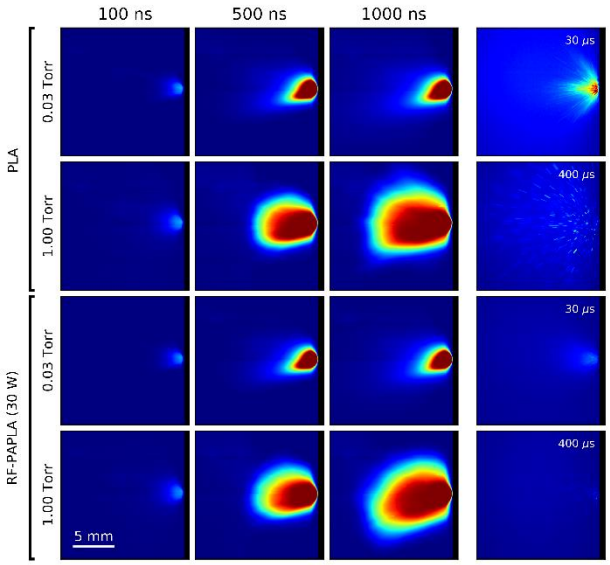

Fig. 3. Laser-induced plasma evolution during PLA and RF-PAPLA processes.

4. Conclusion

High-speed imaging of laser-induced plasma plume expansion during PLA and RF-PAPLA of a titanium target, and SEM imaging of the resulted titanium nanostructures deposited on MWCNTs were performed. The results illustrated the structural variation of the synthesized titanium nanostructures due to the different interaction of the background gas and laser-induced plume at different pressures with/without the presence of the radio-frequency plasma. The droplet ejection process occurring after the plasma-plume expansion was identified as the main cause for the morphological changes observed in the structures synthesizes, when comparing PLA to RF-PAPLA.

5. References

[1] Saha, N.C. and H.G. Tompkins, Journal of Applied Physics, **72**, 7 (1992).
[2] Avasarala, B. and P. Haldar, International Journal of Hydrogen Energy, **36**, 6 (2011).
[3] Avasarala, B. and P. Haldar, Electrochimica Acta, **55**, 28 (2010).
[4] Milošv, I., et al., Surface and Interface Analysis, **23**, 7-8 (1995).
[5] De Giacomo, A., et al., Applied Surface Science, **186**, 1 (2002).
[6] Hordy, N., et al., Carbon, **63**, (2013).
[7] Harilal, S.S., et al., **93**, 5 (2003).